

Persistent homology analysis of protein folding

Takashi Ichinomiya*

*Gifu University School of Medicine,
Yangido 1-1, Gifu, 501-1194, Gifu, Japan and
The United Graduate School of Drug Discovery and
Medical Information Sciences of Gifu University,
Yanagido 1-1, Gifu, 501-1194, Gifu, Japan*

Ippei Obayashi

*Advanced Institute for Material Research,
Tohoku University, 2-1-1 Katahira,
Aoba-ku, Sendai, 980-8577 Japan and
Center for Advanced Intelligence Project, RIKEN,
Nihonbashi 1-chome Mitsui Building, 15th floor,
1-4-1 Nihonbashi, Chuo-ku, Tokyo 103-0027, Japan*

Yasuaki Hiraoka

*Kyoto University Institute for Advanced Study,
Kyoto University, Yoshida Ushinomiya-cho,
Sakyo-ku, Kyoto 606-8501, Japan and
Center for Advanced Intelligence Project, RIKEN,
Nihonbashi 1-chome Mitsui Building, 15th floor,
1-4-1 Nihonbashi, Chuo-ku, Tokyo 103-0027, Japan*

(Dated: May 16, 2019)

Abstract

Developing an understanding of the protein folding process has been an outstanding issue in biophysics. The recent development of molecular dynamics simulation provides insight into this problem; however, the large freedom of motion of the atoms prevents us from understanding of this process. In this study, we apply persistent homology, one of the emerging methods to analyze topological features in a dataset, to reveal the dynamics of protein folding. We develop a new method that combines persistent homology and non-negative matrix factorization to reduce the degrees of freedom, and we apply it to the molecular dynamics simulation of chignolin. Our method exhibits that this molecule has two stable states and one saddle state, which corresponds to native, misfolded, and transition states. We also find an unfolded state, which is not stable and whose dynamics in the reduced space is very slow. Our method provides new intuitive knowledge of the folding process of this molecule.

* tk1miya@gifu-u.ac.jp

I. INTRODUCTION

Since the proposal of Levinthal’s paradox in 1968, the folding of biomolecules such as proteins has been attracted the interest of numerous scientists[1]. Molecular dynamics (MD) simulation has been contributed to the understanding of its mechanism[2]. However, the atoms in the MD simulation has a large degree of freedom, and we need to extract the essential folding dynamics to comprehend the proteins dynamics. For this purpose, several methods have been proposed, such as principle component analysis(PCA)[3], relaxation mode analysis(RMA)[4], time–structure-based independent component analysis(tICA)[5, 6], and manifold-learning[7].

In these preceding studies, researchers attempted to identify the essential motion related with the large deformation that leads to protein folding. Here, we notice that the definition of ”large deformation” is ambiguous. For example, when we consider a case in which a protein on unfolding forms nearly a straight line, a small bend at the center of the molecule will cause a large dislocation of the atoms at the end of the chain. Therefore, the deformation in Ramachandran’s plot[8] is small, whereas that in the atomic configuration is large. Moreover, the importance of deformations also depends on the structure of the protein. For example, when we consider a small protein that has only one β -sheet, a small change in the bond angles at the hair-pin may break the β -sheet structure, In this case, we regard this small change in the angles as a ”large deformation”. However, if this protein is completely unfolded, then a slight change in the bond angle is not regarded as a ”large deformation”. These simple examples shows the difficulties in defining a ”large deformation” in a protein.

In this paper, we propose using topological data analysis(TDA) to characterize the structure and deformation of a protein. In TDA, we investigate the topological signatures such as loops or vacancies, embedded in a dataset. This approach has yielded successful results in many fields, such as the analysis of folding of an RNA hairpin[9] or gene regulation networks[10]. The use of TDA has several advantages compared to employing the standard tools for protein structure analysis, such as Ramachandran’s plot, the distance matrix, or the cartesian coordinates of atoms. First, it can capture the change in the global structure. Several methods such as Ramachandran’s plot only consider the local properties, such as the bending angle between the bonds. By contrast, ”loops” or ”vacancies” are formed from several atoms, and thus, TDA captures the non-local structure. Second, a change in the

topology strongly depends on the conformation of the atoms. For example, if a protein forms a straight chain, then there are no loops. If a small bend occurs at the center of this chain, then the positions of the atoms at the end of the chain exhibit large dislocations, whereas there are still not changes in the loops. By contrast, a small change in the bond angle at the hair-pin of a β -sheet can break the loops formed by the atoms in the β -sheet. Finally, TDA provides intuitive insights into protein dynamics. We can visualize the emergence and disappearance of loops more clearly than the coordinated motions of atoms.

In this study, for TDA, we apply persistent homology (PH) analysis [11] in this paper. PH is based on algebraic topology in mathematics, and has been applied to many problems in physics, chemistry, biology, and medicine[12–15]. Although PH is a strong tool to analyze non-local structures, it has several weaknesses. First, there are difficulties in understanding the result of PH. In the original PH, we only obtain two values called "birth" and "death" for each loops or cavity. Frequently, these two values are insufficient to understand the physical relevance provided by PH. Recently, Escolar *et al.* have developed to calculate "optimal volume cycles", which enable us to get the atoms that form loops or cavities[16, 17]. This methods is useful to explain the result of PH and has succeeded to reveal the hidden structure in glass and amorphous polymers[13, 15]. Another difficulty of PH lies in the fluctuation in the number of loops. Even if the number of atoms in the same, the number of loops obtained by PH depends on the configuration of the atoms. However, the standard machine-learning techniques, such as PCA or clustering, require that all the input data has a same dimension. To overcome this difficulty, several methods such as vectorization of persistent diagram[18], kernel method[19], and the use of persistence landscapes[20] have been proposed.

In this paper, we propose a new technique to apply machine learning to PH analysis. The key concept is to construct a "topological feature vector" using optimal volume cycles. In this approach, we consider the optimal volume cycles as the "text" that describes the protein structure. Each optimal volume cycle is a collection of simplices (edges or faces), similar to a text being a collection of words. This concept enables the use the text-mining technique. In this study, we apply non-negative matrix factorization(NMF) to reduce the dimensions of the topological feature vectors. We apply this method to a dataset obtained by an MD simulation of chignolin. A previous study showed that this molecule has native, misfolded, unfolded, and intermediate structures [4, 7]. In this research, we performed a full atomic MD simulation of chignolin solved by water. We found that the dynamics in the

reduced space yielded two stable and one saddle fixed points, which corresponds to native, misfolded, and transition states, respectively. The unfolded state did not correspond to a fixed point; however, the dynamics in the unfolded state was extremely slow.

The remainder of the paper is structured as follows: In Sec. II, we describe the method of PH, construction of the topological feature vector, and dimension reduction by NMF. In this section, we also describe the details of the MD simulation of chignolin. In Sec. III, we present the results of the analysis. It is shown that PH provides an intuitive description of the folded, misfolded, transition, and unfolded states. The problems to be solved and future direction of the analysis are discussed in Sec. IV.

II. METHOD

Our analysis process is composed of three procedures. First, we perform the PH analysis and calculate all the loops with their optimal volume cycles. Second, we construct a "topological feature vector", in which the contributions of the edges to the formation of the optimal volume cycles are stored. Third, we reduce the dimension of the dataset using NMF. In the following, we explain each of the above steps.

A. Persistent homology with optimal volume cycles

The general mathematical definition of PH is described in terms of the filtration of simplicial complexes[11] or quiver representation[21]. In this subsection, we only explain degree 1 PH of an α -complex composed of a point cloud, which we use for the analysis of protein folding.

Consider there are n atoms at $p_1 = (x_1, y_1, z_1), p_2 = (x_2, y_2, z_2), \dots, p_n = (x_n, y_n, z_n)$ in a three-dimensional space, as depicted in Fig. 1. The PH of the α -complex can be regarded as a topological structure when we place a ball of radius r at p_1, p_2, \dots, p_n . If $r = 0$, all the balls are disconnected, as shown in Fig. 1(a). As we increase r , the balls coalesce, and a loop emerges at $r = b_1$ (Fig. 1(b)). We call b_1 as the "birth" of this loop, and the three edges: (p_3p_5) , (p_3p_6) , and (p_5p_6) , are the set of edges that most tightly surround this loop, as an "optimal volume cycle". This loop shrinks as r increases, and at $r = d_1$, the loop is fulfilled and disappears, as shown in Fig. 1(c). We call d_1 as the "death" of this loop. We

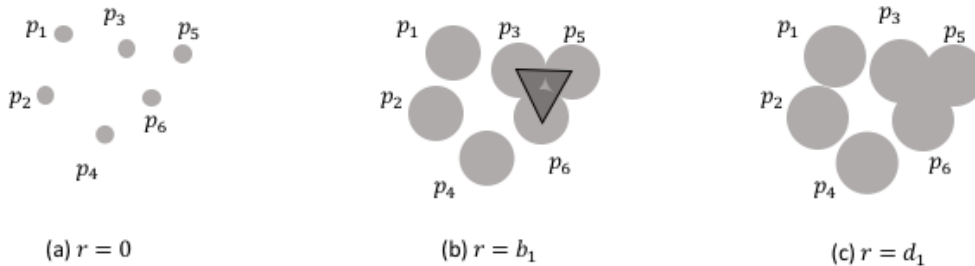


FIG. 1. Example of a persistent homology analysis. If the radius of the balls is 0, then all the atoms are disconnected, as shown in (a). As we increase the size of the balls, the balls coalesce, and at $r = b_1$, we obtain a loop, which is surrounded by three edges, (p_3p_5) , (p_3p_6) , and (p_5p_6) . This loop is destroyed when we increase the size of the balls to $r = d_1$, as shown in (c).

frequently call loops that emerge in PH as "generators".

From one conformation of the atoms, we obtain several loops. As we have mentioned in Sec. I, the number of generators strongly depends on the configuration of the atoms. Even if the number of atoms is the same, the number of generators can be different. This fact has made it difficult to combine a machine-learning technique with PH. In this study, we overcome this difficulty by introducing a "topological feature vector" composed of the optimal volume cycles, which is explained in the next subsection. The calculation of births, deaths, and optimal volume cycles is performed by HomCloud ver.1.2.1[22].

B. Construction of topological feature vector

Using the information of the loops, we define a "topological feature vector," \mathbf{v} , which describe the topology of the point clouds as follows: First, for each edge, $(p_i p_j)$, we list the generators, g_k , whose optimal volume cycles include it. Second, we calculate the "importance" of an edge, $(p_i p_j)$, as the sum of the deaths of g_k . This process is depicted in Fig.2.

This construction of the feature vector is similar to that of a "bag-of-words" and "term frequency-inverse document frequency", which are standard methods used in natural language processing[23]. In these methods, we regard a document as a multiset of terms and

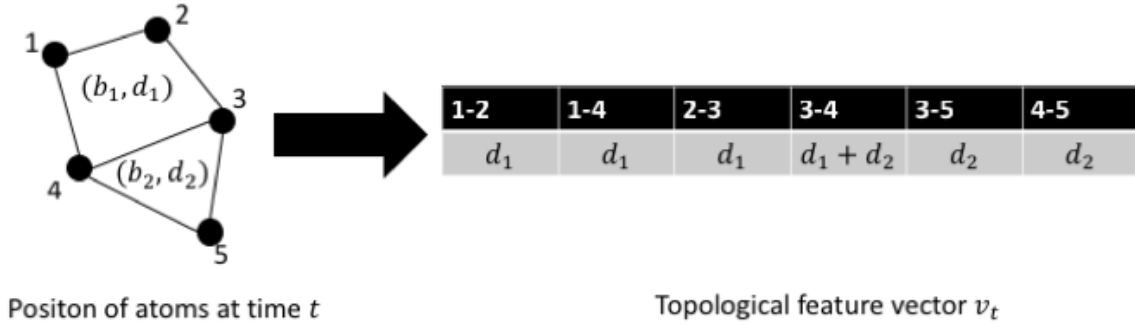


FIG. 2. Schematic description of the topological feature vector.

calculate the "importance" of each term. In our approach, edges play the role of the terms that describe the shape of protein.

We note that there are several possible methods to construct a topological feature vector from the optimal volume cycles. For example, we can create another topological feature vector using births instead of deaths. In this study, we used the death time as the weight of the topological feature vector because a loop with a large death is supposed to represent the large scale structure of a protein. We tested using births instead of deaths; this yielded qualitatively the same result as the one described in Sec. III. Alternatively, we can use the products of deaths instead of sums of deaths. In this study, we use sum of the deaths for simplicity. Indeed, there may be more a complex and sophisticated definition of the topological feature vector. We will discuss this issue in Sec. IV.

C. Dimension reduction by non-negative matrix factorization

The dimension of a topological feature vector is generally high, and dimension reduction with methods such as PCA is useful. In this study, we employ NMF to reduce the dimension of the topological feature vectors[24]. We assume that the M -dimensional topological feature vector at time $t = t_1, t_2, \dots, t_N$ are $\mathbf{v}_1, \mathbf{v}_2, \dots, \mathbf{v}_N$ respectively. In NMF, we calculate non-negative vectors $\mathbf{h}_1, \dots, \mathbf{h}_L$ and a non-negative matrix $\mathbf{X} = (x_{ij})$ that approximate $\mathbf{v}_i \sim \sum_j x_{ij} \mathbf{h}_j$. This approximation is achieved by minimizing $\|\mathbf{V} - \mathbf{X}\mathbf{H}\|$, where $\|\dots\|$ represents the Frobenius norm.

Compared with PCA, NMF has an advantage that the interpretation of the result is easy. In PCA, the component of the basis and coefficients can be negative, and we frequently have the difficulty to understand the meaning of negative coefficients. On the other hand, NMF requires that all the basis and coefficients to be non-negative. Therefore, the basis obtained by NMF is supposed to be the parts of our datasets, and every data is recognized as the weighted sum of these parts.

We note that the decomposition of NMF is not unique. Suppose that \mathbf{X} and \mathbf{H} are non-negative matrices. If both \mathbf{A} and \mathbf{A}^{-1} are non-negative matrices, then $\mathbf{X}' = \mathbf{X}\mathbf{A}$ and $\mathbf{H}' = \mathbf{A}^{-1}\mathbf{H}$ are non-negative, and we obtain another decomposition $\mathbf{V} \sim \mathbf{X}'\mathbf{H}'$. In practice, when the feature matrix is sparse, it is known that if we initialize \mathbf{X} and \mathbf{H} by a nonnegative double singular value decomposition, then optimization with coordinate descent solver exhibits a good performance. Because our feature vector is sparse, we applied this initialization and optimization method. This calculation is performed by scikit-learn 0.19.1[25].

D. Molecular dynamics simulation of chignolin

Following the work of Mitsutake and Takano[4], we conducted the MD simulation of aqueous chignolin as follows. We set one chignolin, 2 Na⁺ atoms, and 3674 H₂O molecules in a cube, and set the temperature and pressure as 450K and 1 atm, respectively. After the energy minimization and a 50–ns equilibration, we performed a 1 μ s MD simulation. We captured the snapshot of the molecules every 10 ps and created 100,000 sample data. In this simulation, we used the ff99SB force field and TIP3P models for the water molecules. From each snapshot, we obtained the coordinates of ten C _{α} atoms in chignolin and performed the PH analysis. The simulation was conducted using GROMACS 16.4[26].

III. RESULT

In this study, we performed PH analysis of a point cloud composed of ten C _{α} -atoms in chignolin and reduced the dynamics into 2-dimensional space by NMF. Fig. 3(a) shows the dynamics in the reduced space in the first 100 ns. Clearly, we find that the dynamics can be well described by the hopping between two states. Fig. 3(b) shows the distribution of

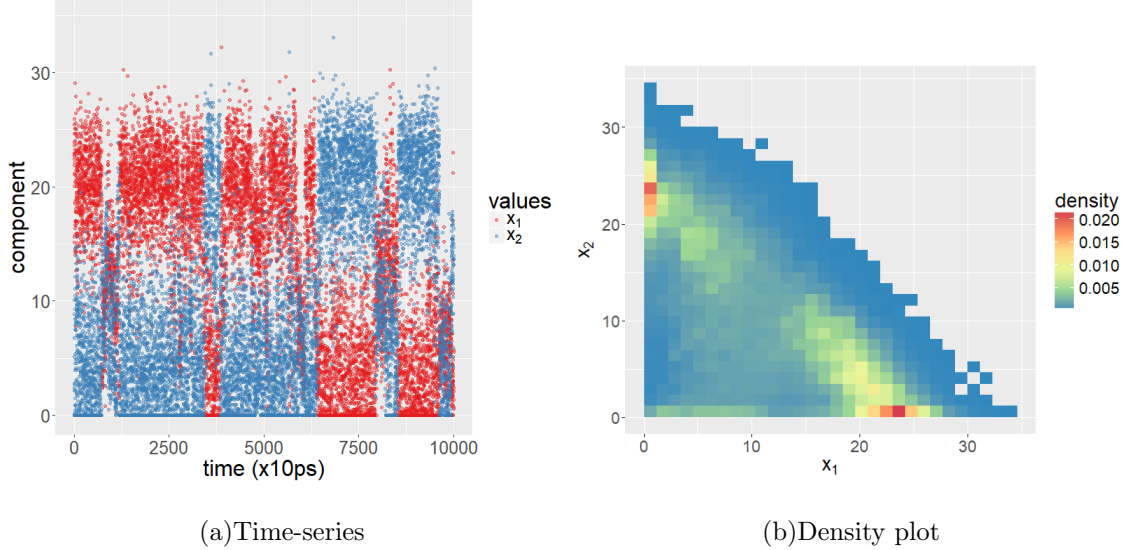


FIG. 3. Dynamics and density of the topological feature vector reduced to a two-dimensional space. (a): Time series from $t = 0$ to 100ns. (b) Density in the reduced space.

the topological feature vectors in the reduced space. We observe that the density has two large peaks at $(x_1, x_2) \sim (25, 0)$ and $(0, 25)$. The density is high along the straight line that connects these peaks, with the minimum at $(x_1, x_2) \sim (10, 15)$. We also note that the density in the area around $(x_1, x_2) \sim (5, 0)$ is also high. The natural interpretation of this figure is the following: the two strong peaks correspond to native and misfolded structures, respectively. The folding path is the straight line that connects these two states. The broad area around $(x_1, x_2) \sim (5, 0)$ corresponds to unfolded state.

To confirm this interpretation, we first examine the vectors, \mathbf{h}_1 and \mathbf{h}_2 , obtained by NMF, as shown in Fig. 4. In the top of this figure, the dark point suggests that the edge between the corresponding amino acids is important for the formation of loops. For example, in the case of \mathbf{h}_1 , the color at the second row-ninth column is dark, which implies that the edge between the corresponding amino acids, Tyr2 and Trp9, makes a large contribution to the formation of the loops. From this figure, first, we note that the adjacent pairs of amino acids, such as Gly1–Try2 or Asp3–Pro4, make a large contribution to the formation of the cycles. This is expected because the distances between adjacent amino acids is kept short owing to chemical bonding. Second, there is a large difference between \mathbf{h}_1 and \mathbf{h}_2 on the edges, Try2–Trp9, Try2–Thr8, and Asp3–Gly7. The component of \mathbf{h}_1 is large for Try2–Trp9, and x_1 becomes large if there is a loop whose optimal volume cycle includes Tyr2–Trp9. By contrast, \mathbf{h}_2 has a large weight on the edge between Tyr2–Thr8. Therefore, the configuration

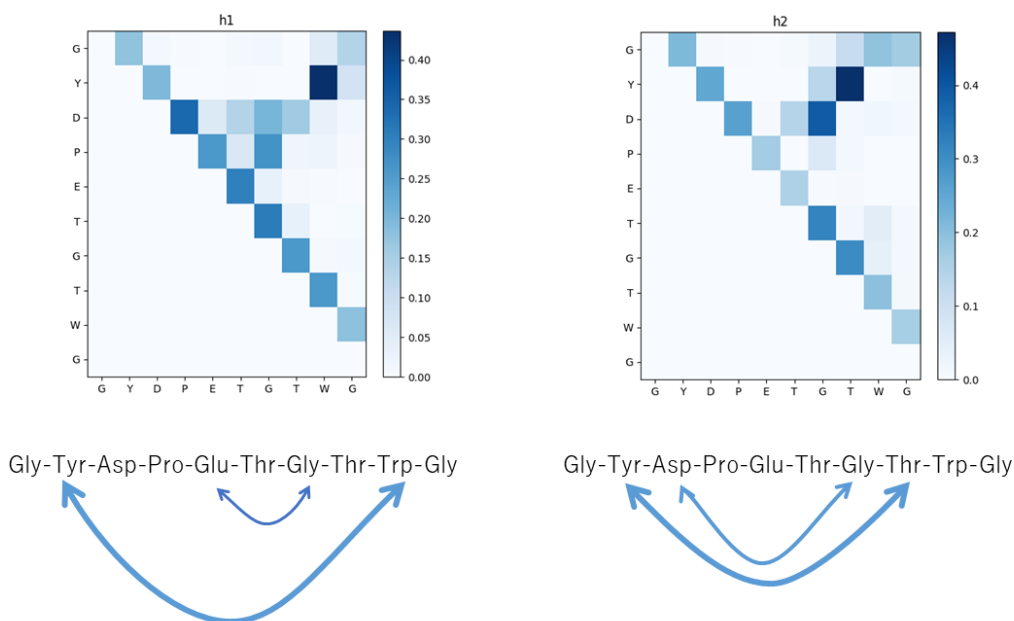


FIG. 4. Components of \mathbf{h}_1 and \mathbf{h}_2 . Top: component of \mathbf{h}_1 and \mathbf{h}_2 . Bottom: Schematic of the coupling that contributes to the feature vector.

that has a large x_2 has a loop whose optimal cycle includes Tyr2–Thr8. These results are depicted in the bottom of this figure. When we apply PH to the native structure, we find that Tyr2–Trp9 is dominant in the native state. Therefore, we conclude that the cluster at $(x_1, x_2) \sim (25, 0)$ corresponds to the native state, whereas that at $(x_1, x_2) \sim (0, 25)$ corresponds to the misfolded state.

Concerned with the state around $(x_1, x_2) \sim (5.0, 0)$, first, we note that a small x_1 and x_2 implies that there are no loops. Because feature vectors \mathbf{v} , \mathbf{h}_1 , and \mathbf{h}_2 are non-negative vectors, the inner product, $\mathbf{v}\mathbf{h}_i = 0$, suggests that $\mathbf{v} = \mathbf{0}$. Therefore we suppose that the state with a small (x_1, x_2) unfolded. This suggestion is supported by the snapshots of molecules. In Fig. 5, we plot examples of the configuration of chignolin in the native, misfolded, and unfolded structures. This figure presents consistent result with our suggestions.

To discuss the transition state, we plot the average flow in Fig.6. This figure is produced as follows: first, we calculate $\delta\mathbf{x}(t) = \mathbf{x}(t + \delta t) - \mathbf{x}(t)$, where $\delta t = 10\text{ps}$. Next, We divide the two-dimensional space into grids of size 1.5×1.5 and calculate the average of $\delta\mathbf{x}(t)$ for each grid. Fig. 6(a) shows the flow in the entire two-dimensional space. Clearly this figure exhibits

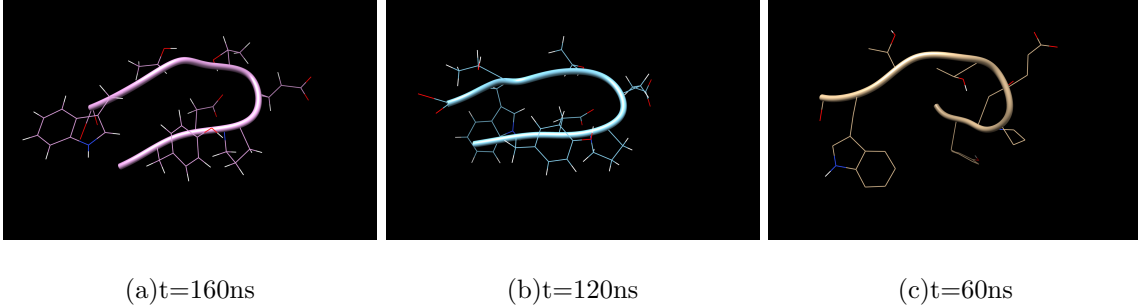


FIG. 5. Example of protein configuration in native, misfolded and unfolded state. (a): native state, $t = 160\text{ns}$, $(x_1, x_2) = (22.7, 3.03)$. (b): misfolded state, $t = 120\text{ ns}$, $(x_1, x_2) = (3.81, 23.1)$. (c): unfolded state, $t = 60\text{ns}$, $(x_1, x_2) = (3.60, 6.44)$

that there are two stable solutions at $(x_1, x_2) \sim (5, 20)$ and $(20, 5)$, respectively. These two stable points correspond to folded and misfolded states, as discussed above. From this figure, we also find that the flow along the line, $x_1 + x_2 \sim 25$, is strong, whereas that at small $x_1 + x_2$ is very weak. To investigate the dynamics in this area more clearly, we plot the flow at $0 \leq x_1, x_2 \leq 15$ in Fig. 6(b). This figure strongly suggests that there is a saddle point at $(x_1, x_2) \sim (12, 12)$. Therefore, this position is supposed to be the transition state. This figure also exhibits that there seems to be no fixed point corresponding to the unfolded state. The flow appears to be weak at $(x_1, x_2) \sim (8.0, 8.0)$, but the flow around this point seems rightward, and it does not seem to be a saddle or stable fixed point. The absence of a stable fixed point in this region suggests that the unfolded state is not meta-stable. Once the chignolin molecule reaches the unfolded state by thermal noise, it remains unfolded for a long time. However, this is not owing to the attraction to the meta-stable unfolded state but because of the slow dynamics in this area.

We conclude this section by comparing our result with previous studies. Mitsutake and Takano applied relaxation mode analysis to reduce the dimension of the physical spaces and found that the conformation of chignolin could be classified into four states: native, misfolded, intermediate, and unfolded[4]. Their result is similar to our results, but there are several important differences. First, they concluded the intermediate and unfolded states as meta-stable states, whereas we deduced they were not. This difference may be owing to the difference in the methods to reduce the dimension and analyze the datasets. Based on the observation of the density of states in the reduced spaces and from the analysis using the Markov model, Mitsutake and Takano claimed that these states are stable. However, as

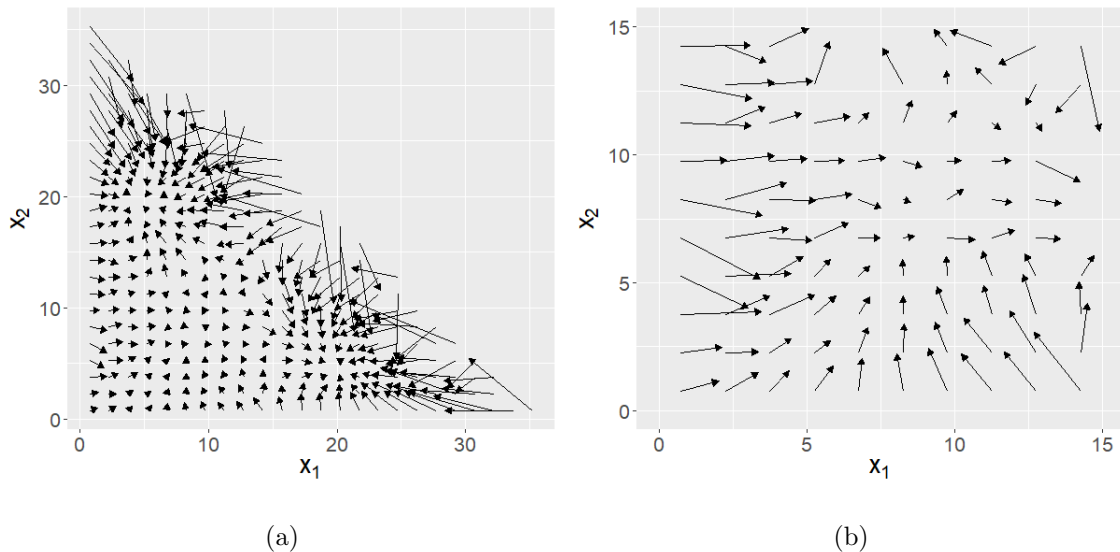


FIG. 6. Average flow $\delta\mathbf{x}(t) = \mathbf{x}(t + \delta t) - \mathbf{x}(t)$. Left: flow in the entire two-dimensional space. Right: flows at $0 \leq x_1, x_2 \leq 15$.

noticed by Frenkel, the density of states depends on the method of dimension reduction[27], and a consistency with Markov model does not guarantee the stability of the intermediate and unfolded states. By contrast, we concluded the instability of the intermediate and unfolded states based on the flow directly, as shown in Fig. 6. Second, Mitsutake and Takano characterized the misfolded state by the hydrogen bonding between Asp3 and Gly7. Fig 4 shows that the contribution of the edge between Asp3 and Gly7 is larger in \mathbf{h}_2 than that in \mathbf{h}_1 , which is consistent with our result. However, our analysis showed that the edge between Tyr2 and Thr8 is more remarkable in \mathbf{h}_2 , which is not mentioned by their work. We need further studies such as PH analysis using all the atoms to determine out the difference between our work and previous studies.

IV. CONCLUSION

In this study, we analyze the folding process of chignolin by persistent homology. By combining PH and NMF, we reduce the dynamics of chignolin into a two-dimensional space. By investigation of the flow in the reduced space, we find that there are two meta-stable states that corresponds to native and misfolded states, one transient state, and one unfolded state. The difference between the two meta-stable state lies in the difference in the edges, Tyr2–Trp9 and Tyr2–Thr8. The unfolded state has no fixed point, but the protein remains

unfolded for a long time owing to the slow dynamics.

The method developed in this study is powerful, but further development is possible. First, we have several approaches to construct the topological feature vector from the optimal volume cycles. In this work, we use the sum of the deaths as the weight of the edge, but we can alternatively also use the sum of births, the product of deaths, or a combination of births and deaths. We have examined that there is no qualitative difference when we use the sum of the births instead of that of the deaths. However, if we analyze the more complex molecules, the result of the analysis may depend on the definition of the topological feature vector. Chignolin is a small molecule having only one β -sheet, with no third structure. If we need to investigate a more complex protein with a third structure, then the definition of the topological feature vector may affect the result of the analysis. Another improvement will be achieved by the selection of the analysis method of the topological feature vector. Once we obtain the topological feature vector, we can apply a lot of data-mining and time-series analysis method, such as hierarchical clustering, PCA, Fourier analysis, RMA, and ICA. Regarding time-series analysis, the application of Markov model will also be promising. The Markov model is a powerful tool for the time-series analysis of protein dynamics[7]. The difficulty in applying Markov modeling lies in the definition of the states. In our study, we have identified unfolded and folded states; however, it is difficult to identify the boundary between them. Application of hidden Markov model(HMM)[28] may solve this problem because this method classify each state automatically. Moreover, we will also be able to apply methods based on text-mining. In our approach, an edge is regarded as a "term" to describe the shape of the protein. In this analogy, the set of generators is document that describes the shape, and the optimal volume cycles are the sentences in the document. Following this analogy, we will be able to use text-mining methods such as topic models or network analysis of terms.

The method we developed in this study is applicable not only to the protein folding problem but other problems in physics, chemistry, and engineering. For example, we will be able to capture the binding of a protein with small molecules, which will contribute to the development of new drugs. Another interesting application of our method is the dynamics of active matter such as school of fish or flocks of birds. Although the dynamics of active matter is keenly studied, its quantitative analysis is difficult. The method we developed in this study will provide insight regarding this problem.

ACKNOWLEDGEMENT

The author thanks to Hiroya Nakao, Hiromichi Suetani, Takenobu Nakamura, Kenji Fukumizu for their fruitful comments. This work is financially supported by JST CREST Grant Number JPMJCR15D3, Japan.

- [1] C. Levinthal, *Journal de Chimie Physique* **65**, 44 (1968).
- [2] T. J. Lane, D. Shukla, K. A. Beauchamp, and V. S. Pande, *Current opinion in structural biology* **23**, 58 (2013).
- [3] A. Kitao, F. Hirata, and N. Gō, *Chemical Physics* **158**, 447 (1991).
- [4] A. Mitsutake and H. Takano, *The Journal of Chemical Physics* **143**, 124111 (2015).
- [5] Y. Naritomi and S. Fuchigami, *The Journal of Chemical Physics* **134**, 65101 (2011).
- [6] C. R. Schwantes, D. Shukla, and V. S. Pande, *Biophysical journal* **110**, 1716 (2016).
- [7] H. Fujisaki, K. Moritsugu, A. Mitsutake, and H. Suetani, *The Journal of Chemical Physics* **149**, 134112 (2018).
- [8] G. Ramachandran and V. Sasisekharan, *Advances in Protein Chemistry* **23**, 283 (1968).
- [9] Y. Yao, J. Sun, X. Huang, G. R. Bowman, G. Singh, M. Lesnick, L. J. Guibas, V. S. Pande, and G. Carlsson, *The Journal of Chemical Physics* **130**, 144115 (2009).
- [10] M. Nicolau, A. J. Levine, and G. Carlsson, *Proceedings of the National Academy of Sciences of the United States of America* **108**, 7265 (2011).
- [11] H. Edelsbrunner, D. Letscher, and A. Zomorodian, *Discrete & Computational Geometry* **28**, 511 (2002).
- [12] K. Xia and G. W. Wei, *International Journal for Numerical Methods in Biomedical Engineering* **30**, 814 (2014).
- [13] Y. Hiraoka, T. Nakamura, A. Hirata, E. G. Escolar, K. Matsue, and Y. Nishiura, *Proceedings of the National Academy of Sciences* **113**, 7035 (2016).
- [14] G. Carlsson, *Acta Numerica* **23**, 289 (2014).
- [15] T. Ichinomiya, I. Obayashi, and Y. Hiraoka, *Physical Review E* **95**, 012504 (2017).
- [16] E. G. Escolar and Y. Hiraoka, in *Optimization in the Real World*, edited by K. Fujisawa, Y. Shinano, and H. Waki (Springer Japan, Tokyo, 2016) pp. 79–96.

- [17] I. Obayashi, *SIAM Journal on Applied Algebra and Geometry* **2**, 508 (2018).
- [18] M. Kimura, I. Obayashi, Y. Takeichi, R. Murao, and Y. Hiraoka, *Scientific Reports* **8**, 3553 (2018).
- [19] G. Kusano, K. Fukumizu, and Y. Hiraoka, in *Proceedings of The 33rd International Conference on Machine Learning* (2016) pp. 1–24.
- [20] P. Bubenik and J. Scott, *Discrete and Computational Geometry* , 1 (2014).
- [21] A. Zomorodian and G. Carlsson, *Discrete and Computational Geometry* **33**, 249 (2005).
- [22] “Homcloud,” <https://www.wpi-aimr.tohoku.ac.jp/hiraoka.labo/homcloud/>.
- [23] C. Manning, P. Raghavan, and H. Schütze, *Introduction to information retrieval* (Cambridge university press, Cambridge, England, 2008).
- [24] D. D. Lee and H. S. Seung, *Nature* **401**, 788 (1999).
- [25] F. Pedregosa, G. Varoquaux, A. Gramfort, V. Michel, B. Thirion, O. Grisel, M. Blondel, P. Prettenhofer, R. Weiss, V. Dubourg, J. Vanderplas, A. Passos, D. Cournapeau, M. Brucher, M. Perrot, and E. Duchesnay, *Journal of Machine Learning Research* **12**, 2825 (2011).
- [26] H. Berendsen, D. van der Spoel, and R. van Drunen, *Computer Physics Communications* **91**, 43 (1995).
- [27] D. Frenkel, *The European Physical Journal Plus* **128**, 10 (2013).
- [28] L. E. Baum and T. Petrie, *Ann. Math. Statist.* **37**, 1554 (1966).